

Electronic Supplementary Information for

# Quantification and Removal of the Carbonaceous Impurity in a Surfactant-Assisted Carbon Nanotube Dispersion and Its Implication to Electronic Properties

*Minsuk Park, In-Seung Choi, and Sang-Yong Ju\**

Department of Chemistry, Yonsei University, 50 Yonsei-ro, Seodaemun-Gu, Seoul 03722, Republic of  
Korea

\* To whom correspondence should be addressed. E-mail: syju@yonsei.ac.kr

Table of Contents .....	S1-2
Absorption cross section calculation of monolayer graphene .....	S3
Defect density calculations of CI and CB.....	S4
Assignment of FT-IR bands .....	S5-6
Fig. S1. UV-vis-MWIR absorption spectrum of CI containing chloroform dispersion .....	S7
Fig. S2. Absorption spectra comparison of CI dispersion in chloroform, CB, and graphene .....	S7
Fig. S3. TEM and SEM images of CI dispersion in chloroform. ....	S8
Fig. S4. CI-subtracted absorption spectrum of FC12-PSWNT dispersion.....	S8
Fig. S5. UV-vis-FIR absorption spectra of FC12 dispersions in <i>p</i> -xylene.....	S9
Fig. S6. AFM height images of acetone-washed HiPco, PSWNT, and LDSWNT .....	S9
Fig. S7. Absorption spectra of vigorous chloroform dispersions .....	S10
Fig. S8. Atomic contents of PSWNT, acetone-washed PSWNT and CI.....	S10
Fig. S9. TGA thermograms .....	S11
Fig. S10. Overall wt. including CI/SWNT and net SWNT purity.....	S11

Fig. S11. Overlaid CI-subtracted net PSWNT spectra .....	S12
Fig. S12. Comparison of AFM-based number of CI per SWNT length.....	S12
Fig. S13. Configuration of prepatterned chip for $\sigma$ and $\kappa$ measurements.....	S13
Fig. S14. Photographs of the transferred PSWNT films on prepatterned chips.....	S13
Fig. S15. CI-added FC12-PSWNT dispersions .....	S14
Fig. S16. Thickness changes of PSWNT films on a quartz substrate by a surface profiler .....	S14
Cited references .....	S15-16

### Absorption cross section calculation of monolayer graphene:

Transmission  $T$  is related to absorption cross-section ( $\sigma_{\text{abs}}$ ) and extinction coefficient or molar absorptivity ( $\varepsilon$ ):

$$T = \frac{I}{I_0} = 10^{-\frac{\sigma l N}{2.3}} = 10^{-\varepsilon l C} = 10^{-A}$$

where  $I_0$  and  $I$  are light intensities before and after passing the sample,  $l$  is path length,  $N$  is number of atom per a given volume,  $C$  is concentration in M. Since unit area of graphene unit cell has two carbon atoms per  $0.052 \text{ nm}^2$ , we know  $N \times l$  value (*i.e.*,  $2/(0.052 \text{ nm}^2)$ ) and  $l$  is thickness of monolayer graphene (*i.e.*,  $0.34 \text{ nm}$ ). In addition,  $T$  of monolayer graphene at  $550 \text{ nm}$  is  $97.7\%$ .<sup>S1</sup>

Rearrangement of the above equation and plugging each value in the equation gives rise to  $\sigma_{\text{abs}}$  of monolayer graphene at  $550 \text{ nm}$ :

$$\begin{aligned}\sigma_{\text{abs}} &= \frac{-2.3 \times \log T}{lN} = \frac{(-2.3) \times (-0.01)}{0.34 \text{ nm} \times \left[ \frac{2}{0.052 \text{ nm}^2 \times 0.34 \text{ nm}} \right]} \\ &= 5.9 \times 10^{-18} \text{ cm}^2\end{aligned}$$

### Defect density calculations of CI and CB:

The defect density, and nature of defects can be estimated by using intensity of D band ( $I_D$ ) and intensity of G band ( $I_G$ ).<sup>S2</sup> The  $I_D/I_G$  can be utilized to express the defect density ( $L_D$ , in nm, average distance between two defects)<sup>S2</sup> by using following equation (the modified Tuinstra-Koenig relation),

$$I_D / I_G = C_A \times \pi(r_A^2 - r_S^2) / L_D^2$$

where  $C_A$  is the dimensionless wavelength-dependent parameter which is given by  $(160 \pm 48) \text{ eV}^4 \times E_L^{-4}$ , and  $r_A$  and  $r_S$  are radius of the area surrounding point defect, and of structurally disordered area, respectively, and  $E_L$  is laser energy in eV.<sup>S2</sup> The  $I_D/I_G$  ratio is 0.267 for CI, and 0.87 for CB<sup>S3</sup>. For both cases, laser wavelength is 532 nm 514.5 nm, respectively, and those values give rise to  $C_A$  of  $5.4 \pm 1.6$  and  $4.7 \pm 1.4$ , respectively. Considering previously determined  $r_A$  and  $r_S$  values (*i.e.*, 3.1 and 1 nm),<sup>S2</sup> the estimated average distance ( $L_D$ ) between defects of CI and CB were approximately 23 and 12 nm. This result indicates that CI possesses higher crystalline graphene than CB.

### Assignment of FT-IR bands:

Combined absorption spectra from UV-vis-MIR and FT-IR measurements reveal profound vibrational bands from solvents (*i.e.*, *p*-xylene, chloroform, and water), FC12, and oxygenated defects of nanocarbons.

In the case of CI dispersions in chloroform (*i.e.*, Fig. S1 for PSWNT-derived dispersion and Fig. S7 for HiPco- and LDSWNT-derived dispersions), vibrational bands originate from both oxygenated defects on CI and chloroform. 1710, 1604, and 1362  $\text{cm}^{-1}$  are observed as strong, weak, and medium intensities and those are assigned to symmetric C=O stretch of carboxylic acid or ketone group ( $\nu_{s, \text{C=O}}$ ), symmetric C=C stretch of aromatic groups ( $\nu_{s, \text{C=C}}$ ), and interaction between O-H bending ( $\delta_{\text{O-H}}$ ) and C-O stretching in phenolic group ( $\nu_{\text{C-O}}$ ), respectively. Those are attributed to oxygenated defects (carboxylic acid, phenol, *etc*) which are also observed in the case of SWNT.<sup>S4-S6</sup> In addition, 3039, 2400, 1519, and 1423  $\text{cm}^{-1}$  which are chloroform-related band appear as noisy features due to absorption saturation as solvent. 3039  $\text{cm}^{-1}$  band stems from symmetric C-H stretching ( $\nu_{s, \text{C-H}}$ ). Other bands originate from either overtones [2400  $\text{cm}^{-1}$  for *ca.*  $2 \times$  C-H symmetric bending ( $\delta_{s, \text{C-H}}$ ), 1519  $\text{cm}^{-1}$  for *ca.*  $2 \times$  C-Cl asymmetric stretching ( $\nu_{\text{as, C-Cl}}$ )] or combination band [1423  $\text{cm}^{-1}$  for symmetric C-Cl stretching ( $\nu_{s, \text{C-Cl}}$ ) + asymmetric C-Cl stretching ( $\nu_{\text{as, C-Cl}}$ )]. Those are in excellent agreement with the literatures<sup>S7, S8</sup> Moreover, 3704  $\text{cm}^{-1}$  band was assigned to symmetric and asymmetric O-H stretches ( $\nu_{s, \text{O-H}}$  and  $\nu_{\text{as, O-H}}$ ) of residual water.<sup>S9</sup> Noisy 2346  $\text{cm}^{-1}$  band was associated with asymmetric C=O stretching ( $\nu_{\text{as, C=O}}$ ) of  $\text{CO}_2$ .<sup>S10</sup> Weak 1474  $\text{cm}^{-1}$  band is tentatively assigned to asymmetric bending of C-H ( $\delta_{s, \text{C-H}}$ ) originating from residue of cleaning solvent (*e.g.*, acetone).

For the cases of FC12-SWNT dispersions (Fig. 3B to 3D and IR extensions (Fig. S5A to S5C) which are the spectra of FC12-HiPco, FC12-PSWNT, and FC12-LDSWNT in *p*-xylene, respectively), more complicated vibrational bands were observed. Vibrational bands consist of the contribution from FC12, oxygenated nanocarbon defects and solvents (*i.e.*, *p*-xylene and residual water). 3409, 3333, and 1705  $\text{cm}^{-1}$  originate from FC12 moiety. The former two bands are attributed to N-H stretches of secondary

amide ( $\nu_{s, R_2N-H}$ ) in the uracil moiety of FC12.<sup>S11, S12</sup> The latter band is corresponding to the  $C_4=O$  stretching of FC12 ( $\nu_{C_4=O}$ ).<sup>S11, S13</sup> Those bands overlaps with bands (*e.g.*, 1717 and 1689  $cm^{-1}$ ) from oxygenated defects (carboxylic acid, quinone, *etc*) of CI and SWNT.<sup>S4-S6</sup> 3704  $cm^{-1}$  band is associated with symmetric and asymmetric O-H stretching ( $\nu_{s, O-H}$  and  $\nu_{as, O-H}$ ) of residual water.<sup>S9</sup> The other noisy features at 3020, 2923, 2730, 1890, 1783, 1630, 1516, 1454, 1043, 795, and 484  $cm^{-1}$  bands originate from *p*-xylene. 3020 (ring C-H stretching,  $\nu_{C-H}$ ), 2923 (symmetric methyl C-H stretching,  $\nu_{s, C-H}$  of methyl), 1516 (ring C=C stretching,  $\nu_{s, C=C}$  of ring), 1454 (methyl scissoring,  $\delta_{s, methyl}$ ), 1043 (methyl rocking,  $\rho_{methyl}$ ), 795 (symmetric ring C-H bending,  $\delta_{s, C-H}$  of ring), and 484  $cm^{-1}$  (ring C-C=C bending,  $\delta_{C-C=C}$  of ring) bands are fundamental vibrations. Other bands are associated from combination bands such as 2730 (in-phase and out-of-phase methyl umbrella), 1890 (ring C=C stretching ( $\nu_{C=C}$ ) and methyl C-C bending, ( $\delta_{C-C}$  of methyl)), 1783 (methyl C-C bending ( $\delta_{C-C}$  of methyl) and methyl asymmetric H-C-H bending ( $\delta_{as, H-C-H}$  of methyl)) and 1630  $cm^{-1}$  (ring C-H bending ( $\delta_{C-H}$  of ring) and symmetric ring C-H bending ( $\delta_{s, C-H}$  of ring)).<sup>S14</sup>

**Fig. S1.** UV-vis-MWIR absorption spectrum of CI containing chloroform dispersion of as-supplied PSWNT. UV-vis-MWIR spectrum (black) was stitched with FT-IR spectrum (blue). Extended biexponential curve to 8000 nm (red) was well agreed with measured curve.

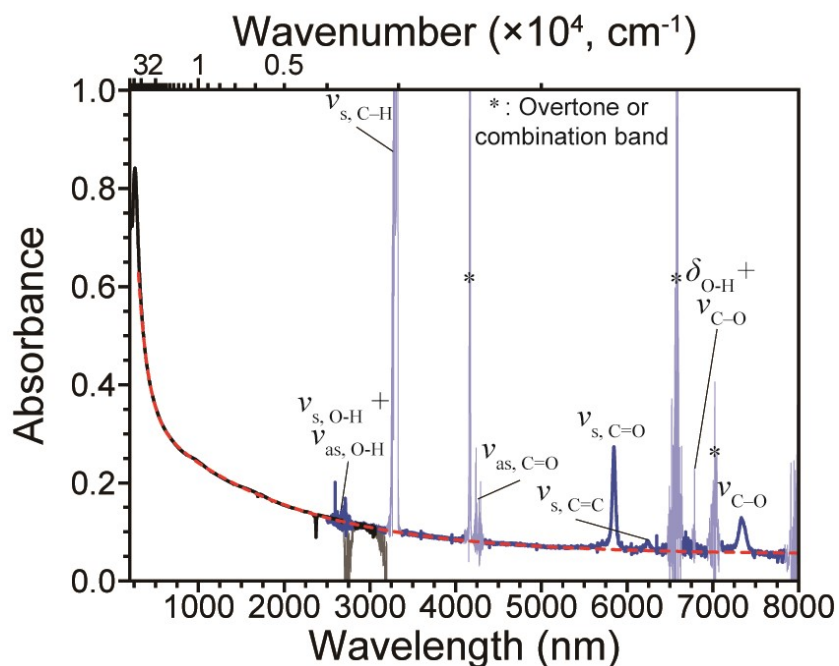


**Fig. S2.** Absorption spectra comparison of (A) CI dispersion in chloroform, (B) CB, and (C) graphene. CB spectra and graphene spectra was adapted with permission from the ref. <sup>S15</sup> and <sup>S16</sup>, respectively. Copyright 2004 American Chemical Society. Copyright 2011 American Physical Society.

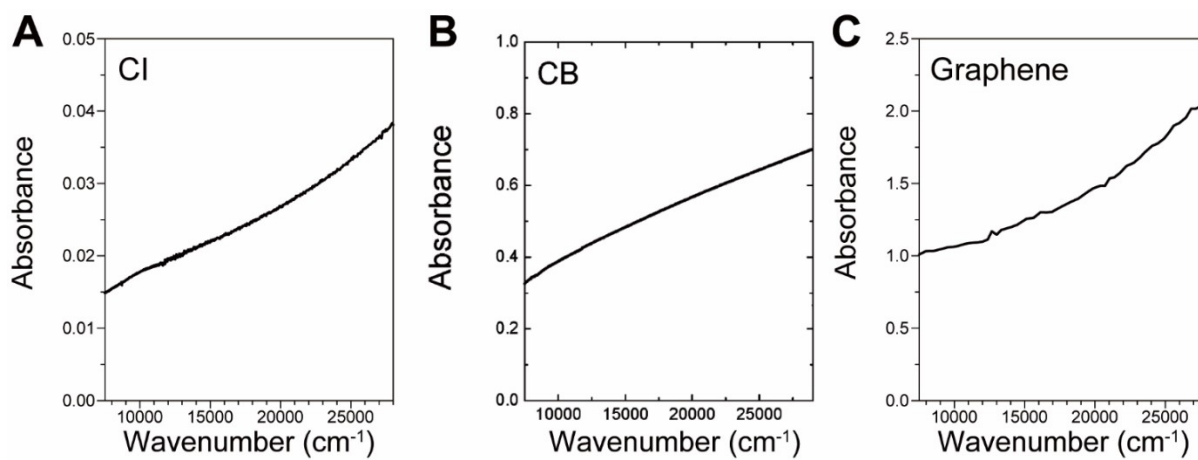


**Fig. S3.** TEM and SEM images of CI dispersion in chloroform. (A) TEM images of CI enriched area and (B) metal catalyst containing area. (C-D) SEM images of concentrated CI enriched sample. A small amount of SWNT is embedded between the CIs.

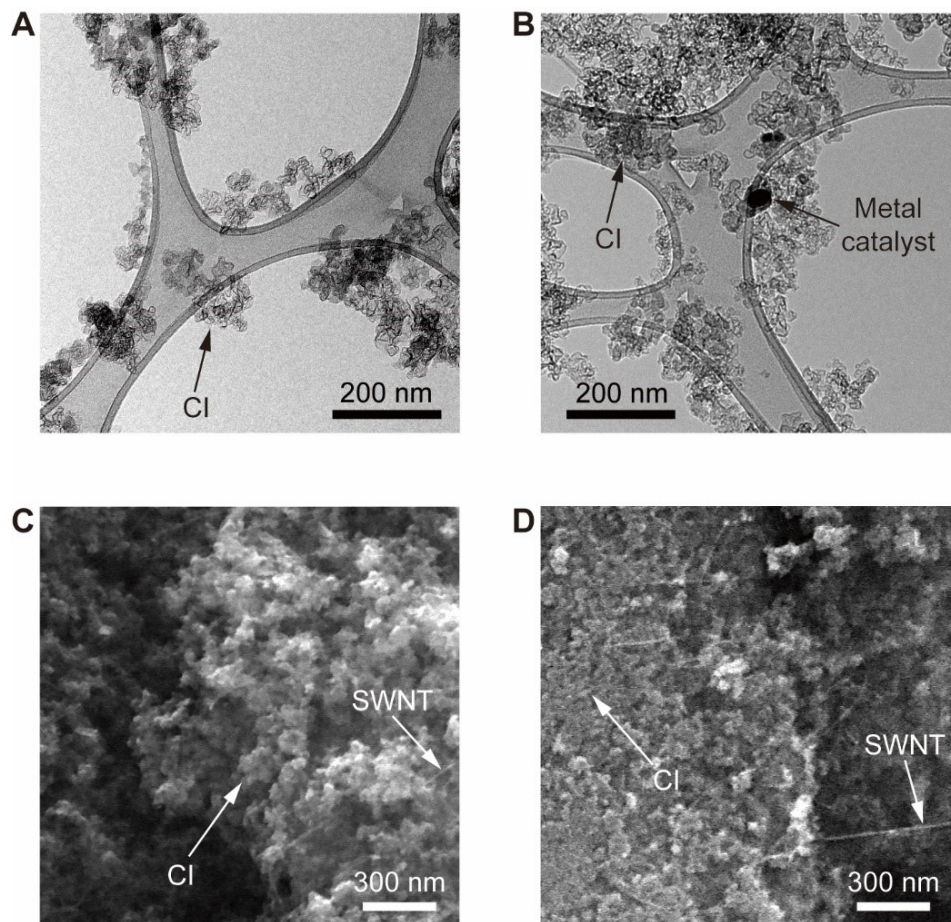


**Fig. S4.** CI-subtracted absorption spectrum of FC12-PSWNT dispersion. Absorption near 2700 nm region stems from symmetric and asymmetric stretches of O-H present in residual water.

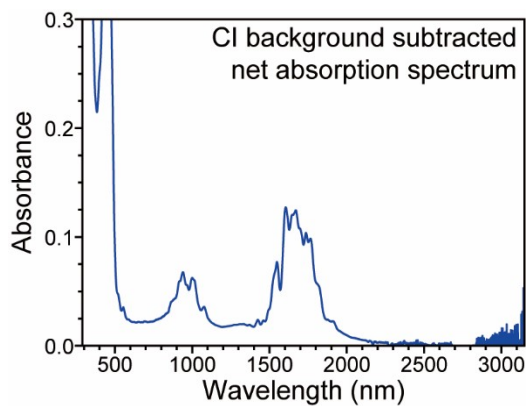




**Fig. S7.** Absorption spectra of vigorous chloroform dispersions from (A) HiPco and (B) LDSWNT samples. Inset: corresponding AFM height images. No SWNT were found in each inset.

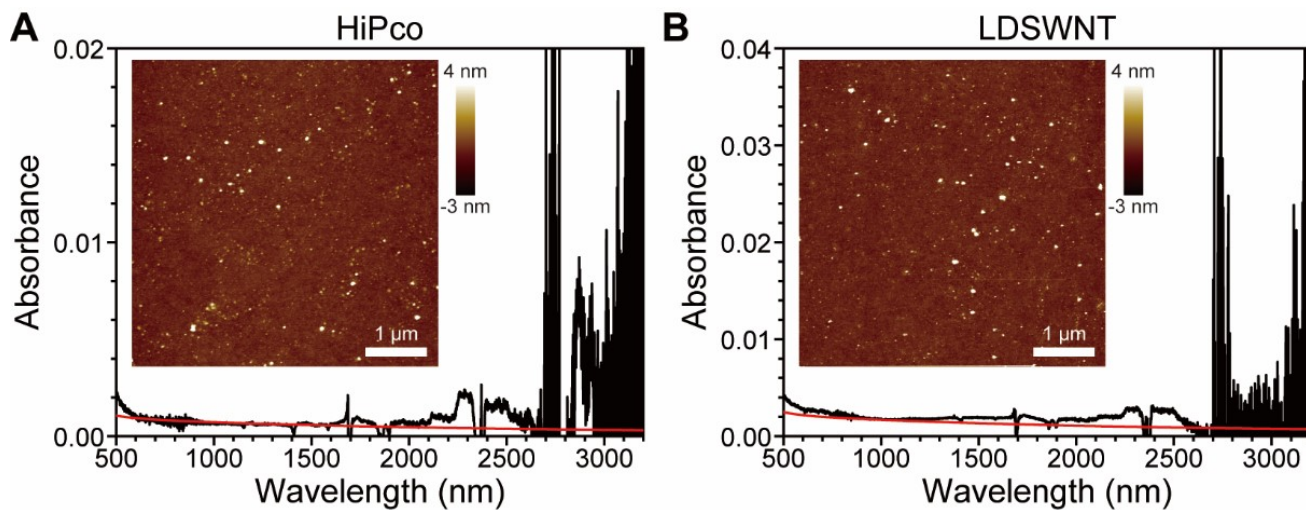


**Fig. S8.** Atomic contents of PSWNT, acetone-washed PSWNT and CI from the dispersions. XPS spectra of (A) PSWNT, (B) acetone-washed PSWNT, and (C) CI samples from the dispersion. (D) Comparison of atomic % present in both samples.

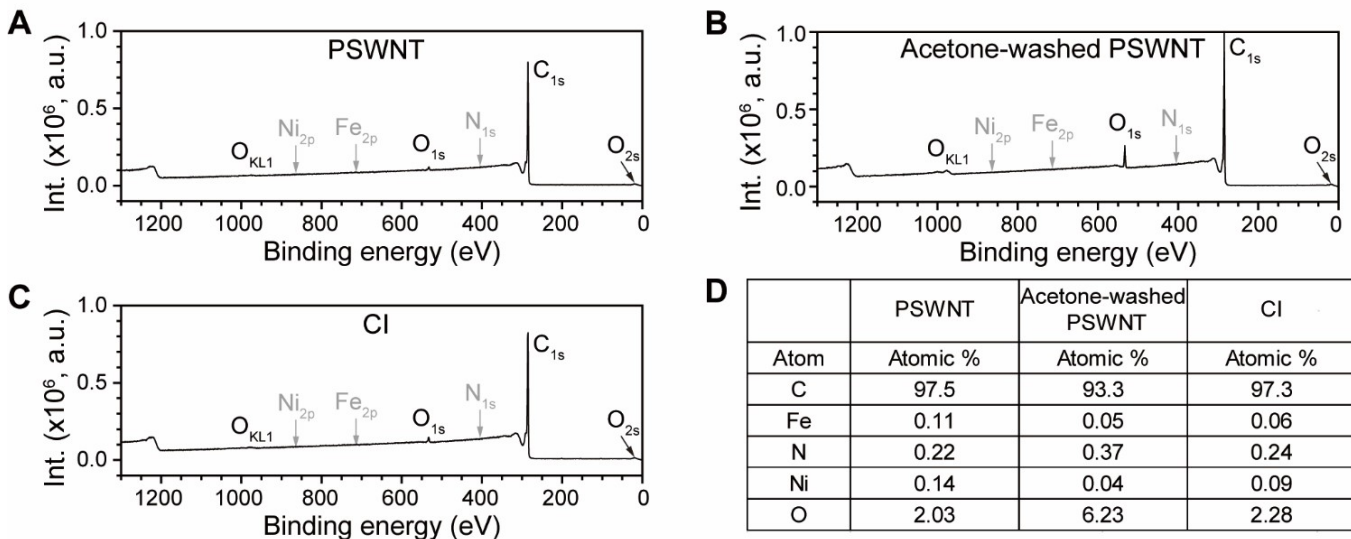


**Fig. S9.** TGA thermograms of (A) PSWNT, (B) CI from CI dispersion in chloroform, (C) acetone-washed PSWNT. (D) Fitting of PSWNT trace with CI trace and acetone-washed PSWNT trace.

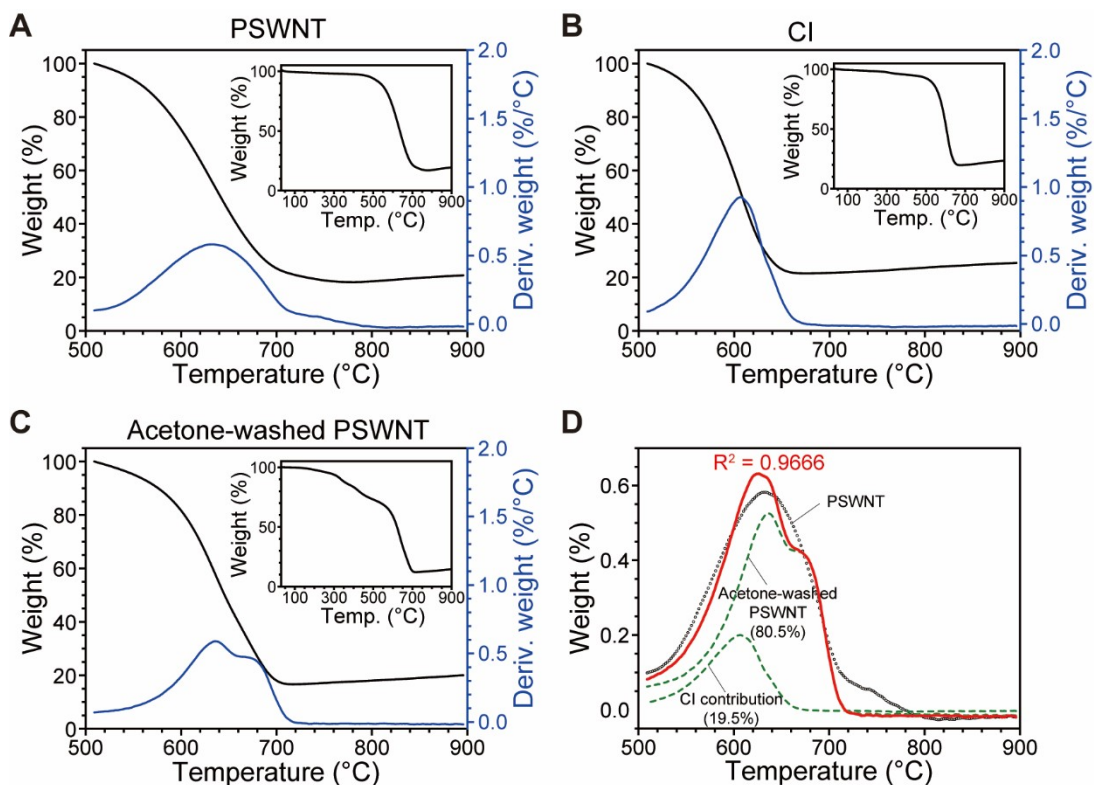


**Fig. S10.** Overall wt. including CI/SWNT and net SWNT purity according to repetitive chloroform extraction cycles. Error bars in overall wt. denotes the minimum digit of microbalance.

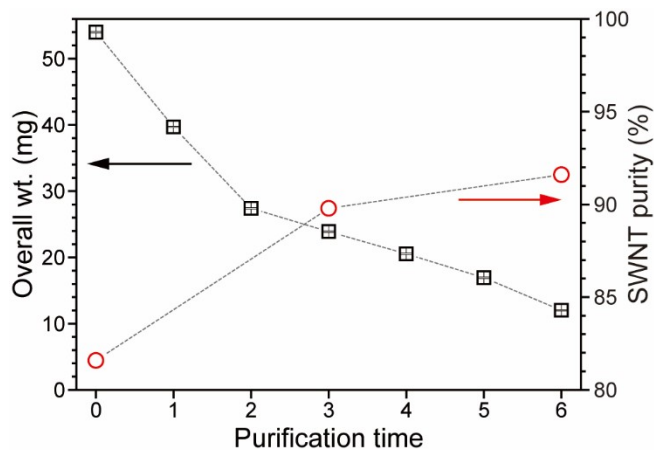


**Fig. S11.** Overlaid CI-subtracted net PSWNT spectra from repetitive chloroform extraction samples such as without chloroform extraction (black), 3 times chloroform extraction (red), and 6 times chloroform extraction (blue) samples.

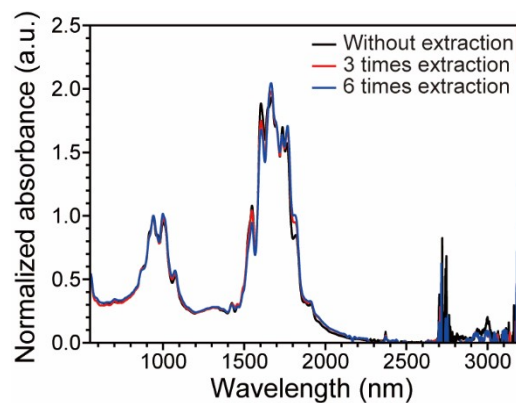


**Fig. S12.** Comparison of AFM-based number of CI per SWNT length according to number of chloroform extraction. Dashed line denotes the number of CI per SWNT length from AFM topography of SPSWNT dispersion. Error bars were obtained from standard deviation using 4 topographies per each sample, and number of CI per SWNT length value of each topography are drawn in grey circle.

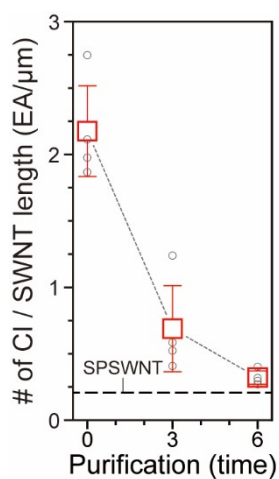


**Fig. S13.** Configuration of prepatterned chip for  $\sigma$  and  $\kappa$  measurements. (A) Photograph of whole prepatterned chip. Dashed box denotes a designated area for materials to be transferred. (B) Low-magnification optical microscope (OM) image of area measuring thermal properties. (C) Zoomed-in OM image of  $\kappa$  measuring circuits on  $\text{Si}_3\text{N}_4$  membrane. (D) Cross-sectional schematic of  $\kappa$  measuring circuits in prepatterned chip. Note that Pt heating wire suspended on a  $\text{Si}_3\text{N}_4$  membrane was used to minimize  $\kappa$  of materials other than sample.<sup>S17</sup>

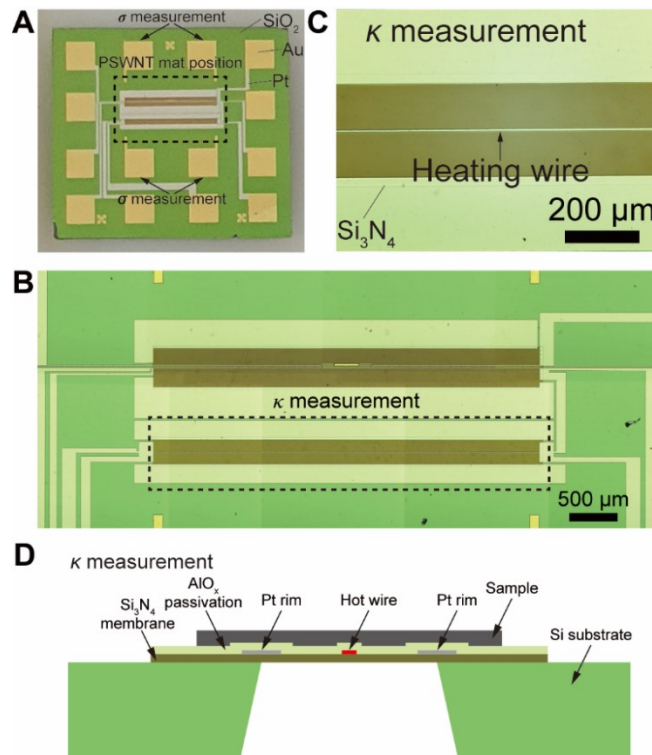


**Fig. S14.** Photographs of the transferred PSWNT films on prepatterned chips with varying CI wt.%. (A) 18.5, (B) 31.2, (C) 53.1, and (D) 69.3.

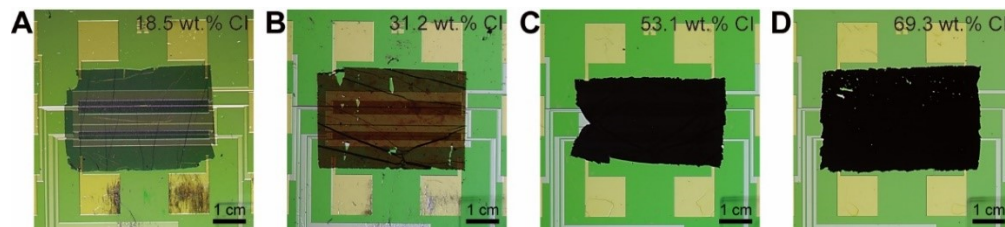


**Fig. S15.** CI-added FC12-PSWNT dispersion. UV-vis-MIR absorption spectra of FC12-PSWNT dispersions in *p*-xylene with varying CI amount. Inset: photograph of the dispersions.

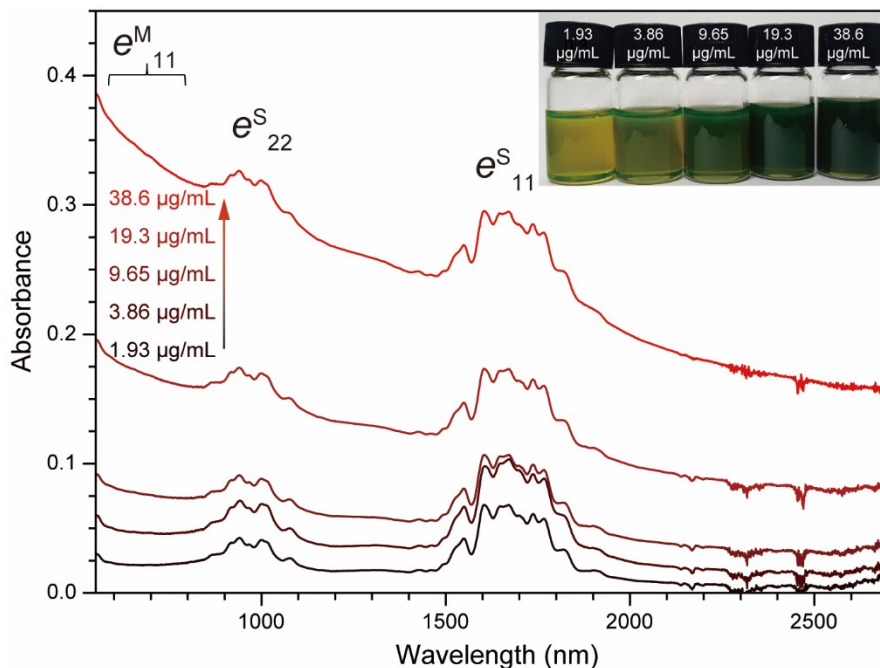
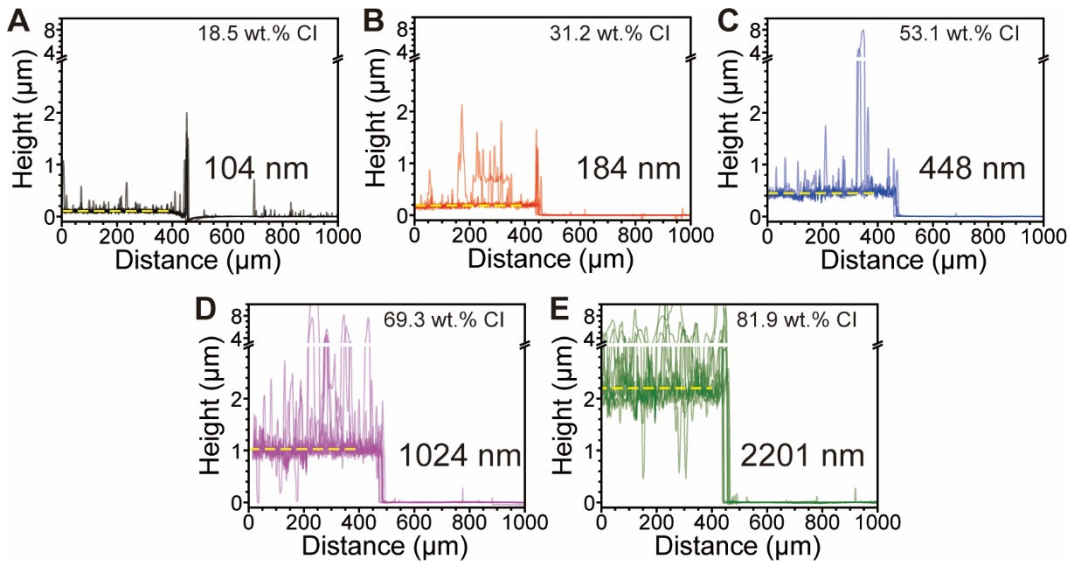


**Fig. S16.** Thickness changes of PSWNT film on a quartz substrate by a surface profiler. Height profiles of PSWNT films with CI whose CI wt. % are (A) 18.5, (B) 31.2, (C) 53.1, (D) 69.3, and (E) 81.9. Average thickness (dashed line) was obtained from basal plane thickness from 5 different measurements.



## Cited references

- S1. R. R. Nair, P. Blake, A. N. Grigorenko, K. S. Novoselov, T. J. Booth, T. Stauber, N. M. R. Peres and A. K. Geim, *Science*, 2008, **320**, 1308-1308.
- S2. L. G. Cançado, A. Jorio, E. H. M. Ferreira, F. Stavale, C. A. Achete, R. B. Capaz, M. V. O. Moutinho, A. Lombardo, T. S. Kulmala and A. C. Ferrari, *Nano Lett.*, 2011, **11**, 3190-3196.
- S3. M. Pawlyta, J.-N. Rouzaud and S. Duber, *Carbon*, 2015, **84**, 479-490.
- S4. A. Kuznetsova, I. Popova, J. T. Yates, M. J. Bronikowski, C. B. Huffman, J. Liu, R. E. Smalley, H. H. Hwu and J. G. Chen, *J. Am. Chem. Soc.*, 2001, **123**, 10699-10704.
- S5. J. Zhang, H. Zou, Q. Qing, Y. Yang, Q. Li, Z. Liu, X. Guo and Z. Du, *J. Phys. Chem. B*, 2003, **107**, 3712-3718.
- S6. U. J. Kim, C. A. Furtado, X. Liu, G. Chen and P. C. Eklund, *J. Am. Chem. Soc.*, 2005, **127**, 15437-15445.
- S7. T. G. Gibian and D. S. McKinney, *J. Am. Chem. Soc.*, 1951, **73**, 1431-1434.
- S8. D. Kurzydłowski, T. Chumak and J. Rogoża, *Crystals*, 2020, **10**.
- S9. J. E. Bertie, M. K. Ahmed and H. H. Eysel, *J. Phys. Chem.*, 1989, **93**, 2210-2218.
- S10. X. Zhang and S. P. Sander, *J. Phys. Chem. A*, 2011, **115**, 9854-9860.
- S11. M. Abe and Y. Kyogoku, *Spectroc. Acta A*, 1987, **43**, 1027-1037.
- S12. S.-Y. Ju and F. Papadimitrakopoulos, *J. Am. Chem. Soc.*, 2008, **130**, 655-664.
- S13. M. P. Kabir, Y. Orozco-Gonzalez, G. Hastings and S. Gozem, *Spectroc. Acta A*, 2021, **262**, 120110.
- S14. R. Lindenmaier, N. K. Scharko, R. G. Tonkyn, K. T. Nguyen, S. D. Williams and T. J. Johnson, *J. Mol. Struct.*, 2017, **1149**, 332-351.
- S15. B. Zhao, M. E. Itkis, S. Niyogi, H. Hu, J. Zhang and R. C. Haddon, *J. Phys. Chem. B*, 2004, **108**, 8136-8141.
- S16. K. F. Mak, J. Shan and T. F. Heinz, *Phys. Rev. Lett.*, 2011, **106**, 046401.

S17. Linseis, TFA - Thin Film Analyzer from LINSEIS, <https://www.linseis.com/en/products/thin-film-analyzer/tfa-thin-film-analyzer/#description>, (accessed 2021/10/20, 2021).